Joule

CellPress

Article

Overcoming ionic migration in perovskite solar cells through alkali metals

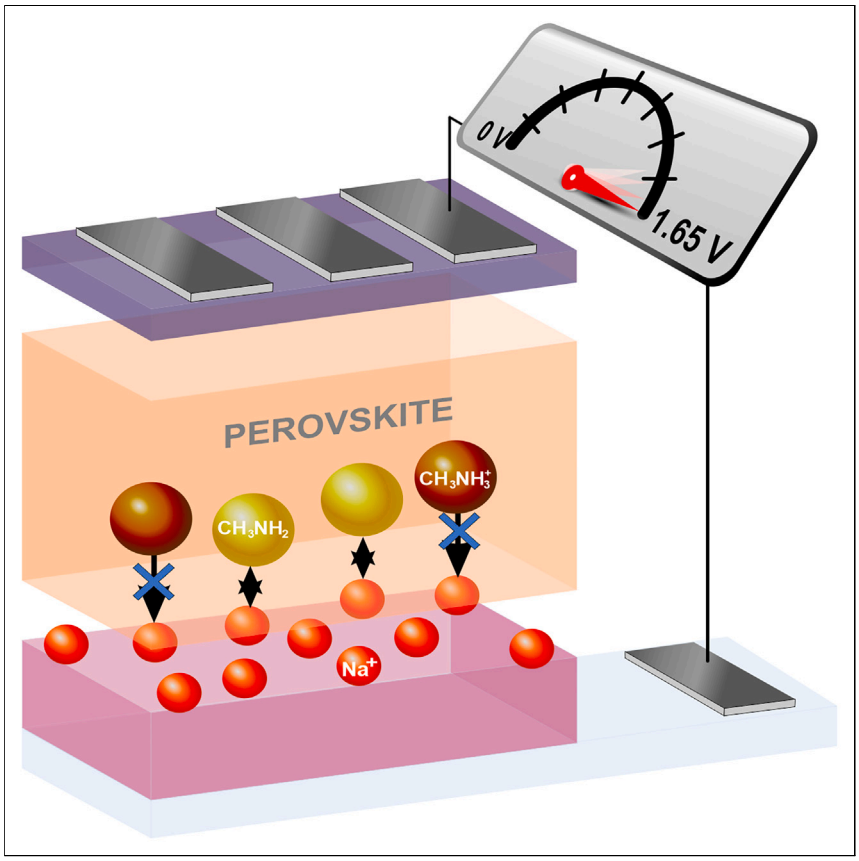

The main bottleneck to achieving an industrial market of solar cells based on perovskite material is the recombination mechanisms provoked by its intrinsic ionic migration. This ionic migration directly affects photovoltage values, diminishing the efficiency and stability of these devices. We use Na^+ to reduce this ionic migration, allowing us to achieve a 1.65 V for a material with a 2.3 eV band gap. The ionic motion is decreased by an electrostatic interaction between the Na and methylamine compounds present in the perovskite bulk.

Clara A. Aranda, Agustin O. Alvarez, Vladimir S. Chivrony, Chittaranjan Das, Monika Rai, Michael Saliba

clara.alonso@ipv.uni-stuttgart.de (C.A.A.)
michael.saliba@ipv.uni-stuttgart.de (M.S.)

Highlights

Alkali metals as additives at the interface in PSCs increase V_{oc}

V_{oc} increases due to a decrease in recombination responsible for IH and NC

Na^+ modulates ionic motion in PSCs, reaching 1.6503 V for a 2.3 eV band-gap material

Ionic modulation is made by electrostatic interaction between Na and methylamine

Aranda et al., Joule 8, 241–254
January 17, 2024
https://doi.org/10.1016/j.joule.2023.11.011

Joule

CellPress

Article

Overcoming ionic migration in perovskite solar cells through alkali metals

Clara A. Aranda,[1,2,3,5,*] Agustin O. Alvarez,[3] Vladimir S. Chivrony,[4] Chittaranjan Das,[1] Monika Rai,[1] and Michael Saliba[1,2,*]

SUMMARY

Alkali metals, as additives in perovskite solar cells (PSCs), have been extensively investigated for their impact on performance enhancement. This performance is sensitive to ion-driven interfacial recombination processes that lead to voltage losses and perform with negative capacitance features in impedance spectroscopy (IS). In this study, we exploited negative capacitance as a tool to systematically investigate the influence of Li, Na, and K on the photovoltage of the wide band-gap material $MAPbBr_3$, known for historical photovoltage losses. Sodium cations were found to mitigate adverse interfacial recombination pathways, yielding a remarkable stabilized open-circuit potential of 1.65 V. Impedance measurements indicated sodium significant influence within the material's bulk, corroborated by time-of-flight secondary ion mass spectrometry and X-ray photoelectron spectroscopy. These techniques confirmed the ability of Na to decrease ionic migration in perovskite materials. X-ray photoelectron spectroscopy (XPS) revealed the underlying mechanism by which Na accomplishes this task: through an electrostatic interaction with the organic compounds.

INTRODUCTION

The stability challenges in perovskite solar cells (PSCs) during operational conditions are a major bottleneck toward commercialization. The main process responsible for this instability is the migration of ionic species present in the well-known ABX_3 structure (A: organic cation, such as methylammonium MA^+, B: metal cation such as Pb^{2+}, and X: halides, such as Cl^-, Br^-, and I^-). These migrating ions lead to detrimental hysteretic responses during current-voltage (*jV*) measurements, coupled with positive capacitance and negative capacitance (NC) in the impedance spectra.[1–3] This also reduces the open-circuit voltage (V_{oc}) significantly compared with established materials such as GaAs or Si.[4] Such losses are caused by the additional recombination pathways introduced by the perovskite ions.[5,6]

Many strategies have been reported trying to mitigate perovskite ion migration, with the improvement in stability and power conversion efficiency (PCE) as consequences. One approach has been the introduction of alkali metals as dopants, both in the bulk and at the interfaces of perovskite devices. The introduction of Cs and Rb as additional cations in the perovskite formulation has become a turning point for creating perovskite compositions via combinatorics, leading, e.g., to the triple cation formulation $Cs_x(MA_{0.17}FA_{0.83})_{(100x)}Pb(I_{0.83}Br_{0.17})_3$, with and without Rb incorporation (RbCsMAFA). Cs stabilized the alpha phase of formamidinium compounds, pushing the stabilized efficiency up to 21% while also enhancing stability

CONTEXT & SCALE

Ion-driven processes influence the performance of perovskite solar cells (PSCs) at the interfaces, leading to voltage losses and generating negative capacitance in impedance spectroscopy (IS). The advantages of alkali metals as additives in PSCs have been extensively studied, but the mechanism behind their beneficial effects was unclear. Our systematic study delved into the effects of Li, Na, and K on a wide band-gap perovskite material, $MAPbBr_3$, known for its photovoltage losses. Among these alkalis, Na has emerged as a standout performer, stabilizing the open-circuit potential at an impressive 1.65 V. Sodium's influence extended beyond the device interfaces, effectively curtailing the migration of perovskite ions at the bulk. The mechanism behind this improvement is an electrostatic interaction between sodium and methylamine compounds. This interaction enhances performance and offers insights into the nuanced behavior of perovskite materials when influenced by specific elements.

and reproducibility.[7] In addition, Rb reduced the loss in potential as low as 0.39 V, and it has been elucidated recently as a blocking agent of diffusion pathways along grain boundaries.[8] This opened the prospect for other alkali metals to be explored.[9] Park and co-workers reported the benefits of K on the perovskite performance when added as a dopant to the perovskite formulation $(FAPbI_3)_{0.875}(CsPbBr_3)_{0.125}$.[10] It was demonstrated that the role of K was shown to have bulk-directed effects. Its bulk effects were analyzed by *in situ* photoluminescence (PL) measurements, showing a moderate reduction in the intrinsic ionic migration, with a drastically reduced hysteretic response from 0.2 to ~0. A drop in the kinetic formation of the ionic double layer was concluded with lower capacitance values at intermediate frequencies.[11,12] This analysis, however, was not performed in a complete device, but in an interdigitated substrate with symmetric configuration, metal/perovskite/metal, to remove the effects of selective contacts.[13]

The beneficial effect that alkali metals have on the performance of perovskite cells is therefore evident, being used even in other non-photovoltaic applications such as light-emitting diodes (LEDs) with outstanding results.[14,15] The benefits that alkali metals have on the photovoltaic response of perovskites have also been predicted on the basis of theoretical studies by density functional theory (DFT).[16] However, the experimental alkali metal results are disconnected from each other, with regards to doping place, composition, and effects. This makes the mechanisms responsible for the beneficial impact of alkali metals difficult to unravel.

In our previous studies, we focused on investigating the impact of lithium (Li) cations as dopants at the interface between the electron transport layer (ETL) and the perovskite material (PVK) on the photovoltage of solar cells. By using a wide band-gap material, specifically methylammonium lead bromide, $MAPbBr_3$, which is known to exhibit significant photovoltage losses, we demonstrated that the presence of Li^+ at the interface reduces the accumulation of holes, resulting in reduced recombination and an increase in the V_{oc} of $MAPbBr_3$ cells, reaching up to 1.58 V.[17] In a subsequent study, we conducted a comprehensive analysis of the *jV* curves of these Li-doped cells at various scan rates and conducted an in-depth investigation of the impedance responses. Notably, we were the first to establish a connection between the occurrence of inverted hysteresis (IH) and NC characteristics, which are associated with the accumulation of ionic species at the ETL/perovskite interface.[18] We demonstrated that the presence of Li^+ can significantly reduce or even completely eliminate the NC features by effectively reducing recombination mechanisms associated with this phenomenon. Through these two studies, we established that the presence of Li^+ at the ETL/perovskite interface can effectively mitigate photovoltage losses in $MAPbBr_3$ cells by suppressing recombination processes related to NC and IH characteristics.

In this work, we are going one step further trying to decipher completely the mechanism of action of the alkali additives and how exactly they can reduce the recombination processes related to perovskite ionic accumulation affecting V_{oc} values. By systematically adding three alkali salts containing bis(trifluorometilsulfonil)amina—Li-TFSI, Na-TFSI, and K-TFSI—on the ETL/perovskite interface, we find a distinct impact on the final performance of the cell depending on the used alkali metal. As evidenced by impedance spectroscopy (IS), time-of-flight secondary ion mass spectroscopy (ToF-SIMS), and X-ray photoelectron spectroscopy (XPS), a clear trend of effects is occurring. A stabilized open-circuit potential (OCP) of 1.65 V has been reached at ambient conditions and with no encapsulation when Na is the additive, followed by Li and K. IS analysis revealed that no NC is present for the Na sample,

[1]Institute for Photovoltaics (*ipv*), University of Stuttgart, 70569 Stuttgart, Germany

[2]IEK5-Photovoltaics, Forschungszentrum Jülich, 52425 Jülich, Germany

[3]Institute of Advanced Materials, University Jaume I, Avenida de Vicent Sos Baynat, s/n, 12006 Castelló de la Plana, Spain

[4]Instituto de Ciencia de los Materiales (ICMUV), Universidad de Valencia, C/Catedrático José Beltrán, 2, Paterna 46980 Valencia, Spain

[5]Lead contact

*Correspondence: clara.alonso@ipv.uni-stuttgart.de (C.A.A.), michael.saliba@ipv.uni-stuttgart.de (M.S.)

https://doi.org/10.1016/j.joule.2023.11.011

which is directly related to diminished recombination. Furthermore, a ToF-SIMS depth profile revealed a decrease in the migration of perovskite ions for the Na sample. This effect is coupled with the XPS results, showing a higher binding energy in N s1 spectra for the Na sample. The reduction in the migration capability of perovskite ions generates a cascading effect of benefits impacting bulk and interface, improving hysteresis, stability, and V_{oc}. An interaction between Na and MABr compounds is revealed as the key factor in the reduction of this ionic migration, opening new prospects in the control and understanding of perovskite dynamics.

RESULTS AND DISCUSSION

Design of the experiment

The chosen PVK for this study is $MAPbBr_3$, as previously mentioned. Its wide band gap of 2.3 eV was chosen because the best-reported V_{oc}'s are only at ~1.65 V. Thus, the loss in potential is at ~0.65 eV, which is still far away from the theoretical minimum at 0.3 eV. This means a V_{oc} of 2.0 V is the upper ceiling for a band gap of 2.3 eV. This is in stark contrast to narrow band-gap perovskites where losses-in-potential as low as ~0.3 eV have been reported. Therefore, there is still a significant scope to improve the current state-of-the-art wide-band-gap perovskites, foremost due to its applicability beyond photovoltaics, such as LEDs, or in electrochemical reactions such as water splitting. Moreover, it is a familiar PVK to the authors, as evidenced by previous results discussed in the introductory section of this manuscript, which is another motivation for our choosing this as the model system for this study.

We have used a regular configuration with fluorine-doped tin oxide (FTO) as transparent conductive oxide (TCO), compact and mesoporous TiO_2 as ETL, $MAPbBr_3$ as absorber material, and 2,2′,7,7′-Tetrakis[N,N-di(4-methoxyphenyl)amino]-9,9′-spirobifluorene (Spiro-OMeTAD) as hole transport layer (HTL). The back contact was Au. We use Li-TFSI, Na-TFSI, and K-TFSI (Figure S1A) as sources for the alkali additives to perform a systematic analysis of the alkali effects on photovoltage values. The three salts were deposited in different devices as an extra layer on the mesoporous titanium film by spin-coating, using twice the concentration previously reported by our group, for a more pronounced effect.[17] After deposition, we proceeded to a high-temperature annealing (450°C), following the method described by Heo et al.[19]

The PVK was deposited afterward inside the glovebox with a nitrogen atmosphere. A 1.4 M of precursor solution brings a thick and smooth film after pouring toluene as an antisolvent.

Morphological analysis

We carried out the X-ray diffraction (XRD) analysis (Figure S1B) on the freshly prepared $MAPbBr_3$ films. All the samples, including reference (without alkali treatment), show a very-high crystallinity, containing the main planes corresponding to the cubic system: (100), (200), (300), and (400) at 15°, 30°, 45.8°, and 62.6°, respectively. However, there are no conclusive differences between the distinct samples. Scanning electron microscopy (SEM) analysis (Figure S1C) qualitatively shows that the nature of the alkali dopant can generate slight differences in the morphology and degree of infiltration of the PVK into the doped-mesoscopic TiO_2 layer. In the cross-section images, it can be appreciated how the sample containing Na is more embedded into the mesoporous film. A better infiltration of PVK into the ETL can reduce recombination pathways between the ETL and HTL, which can ultimately improve the performance of the device. However, to confirm this, a poor filling, or a quasi-steady-state photoinduced absorption (PIA) spectroscopy would have to be carried out.

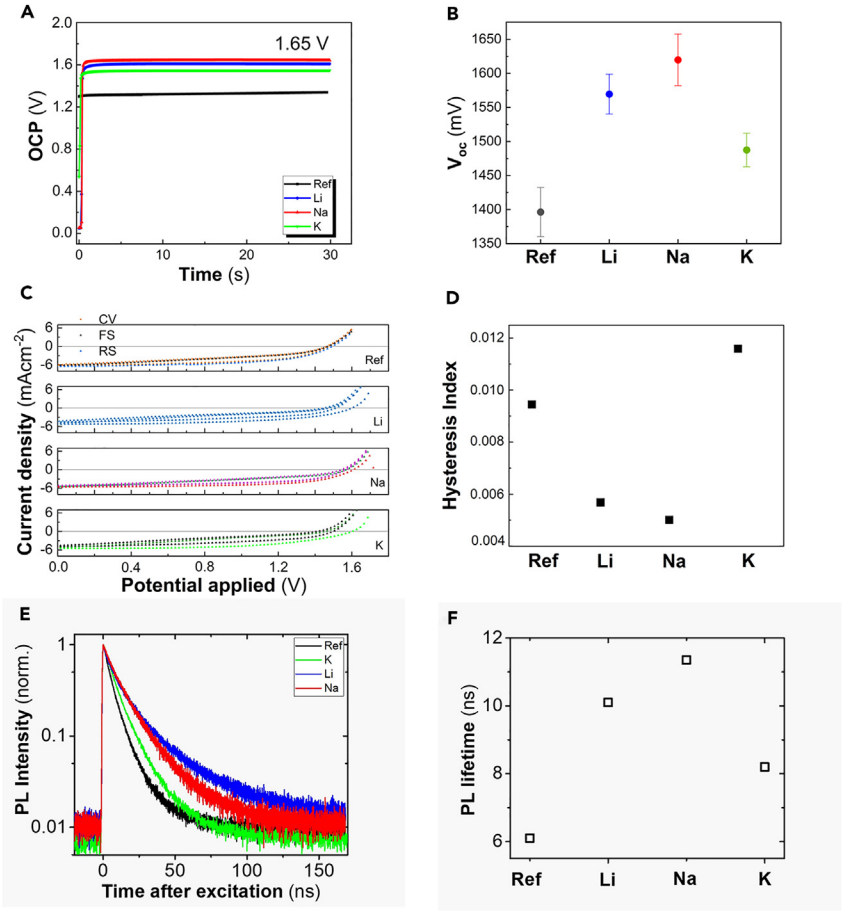

Figure 1. Photovoltaic analysis

(A) Stabilized open circuit voltage measured at ambient conditions without encapsulation.

(B) Distribution of stabilized OCP values obtained from a set of 10 different devices of each type.

(C) *jV* curves showing the reverse scan (maximum V_{oc}, forward scan and a cyclic voltammetry, just after the previous two scans, at 50 mV s^{-1}.

(D) Hysteresis index of the respective samples analyzed.

(E) Time-resolved photoluminescence decay.

(F) Photoluminescence lifetimes of the samples after the monoexponentially fitting of TRPL spectra (see supplemental information for details).

To further characterize the films, UV-vis absorbance measurements were carried out, obtaining the distinctive spectra with the corresponding peak around 540 nm for bromide materials (Figure S2A).[20] The Tauc plot analysis confirms no variation in the band gap at 2.3 eV for all doping types (Figure S2B), indicating that the alkali metals did not cause any lattice change. However, a difference emerges when measuring steady-state PL spectra. All doped samples show an increase in the PL response with respect to the reference (Figure S2C). This matches with our previous work related to Li-doping at the TiO_2 interface, showing a suppression of non-radiative recombination.[17]

Photovoltaic analysis and IS characterization

From previous works,[17] the effect that Li^+ has on the $MAPbBr_3$ PVK directly impacts the OCP and on the cyclic voltammetry (CV) response and impedance behavior. However, we need to confirm whether this effect is just for the Li^+ or whether it can be similar for other alkalis such as Na and K for generality. To check this, we performed an OCP measurement at room conditions and without encapsulation.

Figure 1A shows a champion cell with a stabilized OCP of 1.6503 V for the sample containing Na. This is among the highest reported voltages in literature for any PVK. This value is followed by the Li, K, and the reference devices consecutively, being reproducible on different samples, as shown in Figure 1B.

This increase in the OCP must be related to a reduction of undesired nonradiative recombination mechanisms.

Our time-resolved PL (TRPL) measurements (Figure 1E) show that the luminescence decay kinetics of the studied samples lengthen with doping. Our preliminary analysis of the kinetic data showed that they all fit well by the sum of three exponentials; however, the average lifetimes calculated from the results of such fitting contain a significant contribution from the longer-lived component (a time constant of the order of 50 ns), which is not related to charge recombination and has its source in the photon recycling effect, i.e., multiple re-absorption and re-emission of the PL light in the light-scattering perovskite film (for details, see Note S1 in supplemental information). Since we are interested in comparing exactly the rates of charge recombination for different samples, for such a comparison, we used the time constants obtained by monoexponentially fitting the initial stages of kinetic decay (during the first 5–7 ns, which is comparable to the lifetimes determined in this way). The charge recombination lifetimes of the samples thus obtained were τ(Ref) = 6.1 ns, τ(K) = 8.2 ns, τ(Li) = 10.1 ns, and τ(Na) = 11.35 ns, see Figure S4. Such lengthening of the kinetics upon the addition of alkali metals unambiguously indicates that the presence of alkali metals leads to a decrease in the efficiency of nonradiative recombination due to a decrease in deep trap concentration. Note that the dependence of PL lifetimes on alkali type agrees well with the dependence obtained for V_{oc} (see Figure 1B), which confirms the common nature of these two effects.

CV curves at 50 mV s^{-1} under illumination conditions (1 sun; AM 1.5) are shown in Figure 1C, with corresponding photovoltaic statistics in supplemental information (Figure S6). In Figure 1D, we show, for champion cells, the corresponding hysteresis index (HI), defined by Equation 1:

$$HI = 1 - \frac{PCE_{FS}}{PCE_{RS}} \qquad \text{(Equation 1)}$$

where FS stands for the forward scan (from short circuit to open circuit) and RS for the reverse scan (vice versa). The differences in the hysteretic behavior are evident. The higher the V_{oc}, the lower the HI from 0.01 to 0.005, in the case of Na. A trend that is also matching with the lifetimes of the 4 samples (Figure 1D).

From previous IS works, we know that a direct correlation exists between hysteresis behavior and capacitance values. A normal hysteresis (NH), or positive HI, is correlated with positive capacitance values at low frequencies, the domain that gives information mainly about interfacial processes.[21] In a more recent publication, we reported that NC features and IH have a common origin. In that work, we proposed that these effects are a consequence of the interaction between perovskite ions and interfaces, yielding to a slow recombination mechanism, with a kinetic relaxation time (τ_{kin}) taking values around 10^2 s.[18,22] Afterward, this relation between NC and IH was investigated for other devices, including memristors.[23,24]

Knowing this, if the Na sample is the one showing the highest V_{oc}, it would thereby diminish the interfacial recombination, and this, in turn, would need to be reflected in its impedance spectra.[25–27] Therefore, we performed the IS analysis toward OCP

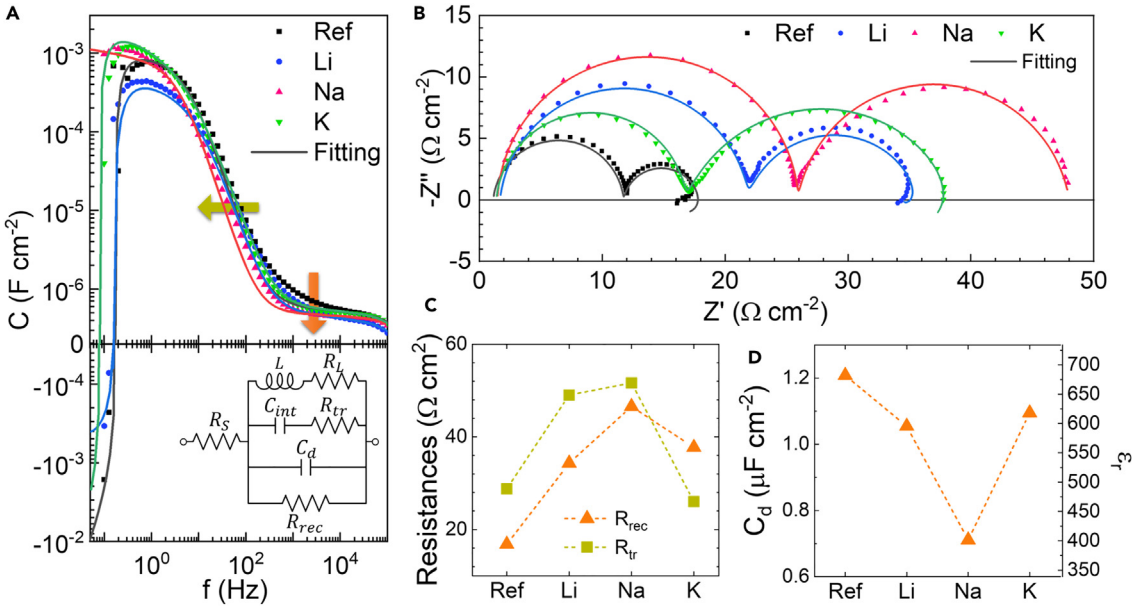

Figure 2. Impedance spectroscopy characterization

(A) Capacitance versus frequency plot.

(B) Impedance spectra (experimental data with dots and fitting with lines) of the samples showing the different resistances.

(C) Fitted resistance values in linear scale. Higher recombination and transport resistance for Na sample.

(D) Dielectric capacitance values together with the dielectric constant for all samples. The trend fits well with the hysteresis behavior.

under 1 sun illumination conditions. It is important to note that this analysis was performed with aged samples (week-old samples) to see a more pronounced interfacial effect. In aged samples, it is easier for the perovskite ions to migrate toward the interface, as we previously established.[18]

Figures 2A and 2B show the impedance spectra response for the four different samples. We note that the spectra response for all the samples presents two well-defined arcs (Figure 2B). Each arc corresponds to a plateau in the capacitance plot in Figure 2A. The first arc is correlated with the high-frequency capacitance plateau (from approximately 10^5–10^2 Hz), and the second arc is correlated with the intermedia-low-frequency capacitance plateau (from approximately 10^1 Hz to 10^{-1} Hz). These two arcs are typically observed in PSCs, and they have been correlated with bulk and interfacial processes, respectively.[28] However, in the case of the Li, K, and Ref samples, at the lowest frequencies, we observe an additional feature, the NC. The NC in Figure 2A, generates an arc below the $-Z'' = 0$ axis in Figure 2B. Interestingly, this is not observed in the Na sample. Again, this feature has been correlated with an extra recombination pathway, which is detrimental to the performance of the device, and we proposed the origin of this feature to the interaction between the perovskite ions/vacancies and the contacts.

To achieve a more detailed comparison between the different impedance spectra, we employed an equivalent circuit (EC) (inset in Figure 2A) to fit each spectrum.[29] The results of the fitting are shown in Figures 2A and 2B with lines of the colors corresponding to the spectra. The complete analysis of fitted parameters is shown in Figure S7. In Figures 2C and 2D, we highlight the most relevant data for our study. The transport resistance (R_{tr}) has been associated with the transport of the perovskite ion/vacancies in the perovskite.[22,29] Interestingly, the trend of R_{tr} in Figure 2C is the inverse of Figure 1D (hysteresis), which is an argument to believe that the ionic

migration is reduced with the addition of alkali metals, especially for the case of Na sample. Previously, Park and co-workers have reported the effect of the K doping on the perovskite bulk. They concluded that this additive reduces ionic migration occurring in the perovskite film.[10] One of their main proofs for this conclusion was the observation of the shift in the capacitance spectra at intermediate frequencies, in the same way, that can be observed for our results here (yellow arrow in Figure 2A).

Another interesting result from the fitting is the difference in the recombination resistance (R_{rec}), associated with the electronic recombination in the bulk material. The differences observed between the samples suggest that the Na sample has lower recombination centers in the bulk (such as defects) than the Li and K samples, which, in turn, have fewer recombination centers than the reference cell.

In addition, the dielectric capacitance (C_d), usually associated with bulk processes occurring at the high-frequency domain,[21,30] changes drastically in the case of the Na sample. For Ref, Li, and K, C_d takes values between 1 and 1.2 (μFcm^{-2}), whereas in the case of the Na sample, it dropped down to 0.7, which would have several implications at the atomic level.

Bulk characterization: ToF-SIMS and XPS analysis

To obtain information about the atomic level and the distribution of the doping additives, a ToF-SIMS study was performed, using layers of the ETL with the alkali additives and $MAPbBr_3$ onto a TCO substrate. The measurements employed a liquid metal ion gun (LMIG) with the following parameters: primary beam: Bi^+, 30 keV, 50 × 50 μm^2, 128 × 128 $Pixel^2$, positive polarization. Secondary beam: Cs, 1 keV, 200 × 200 μm^2, 5 frames. To minimize sputter and surface charging effects on signal intensity, measured signals were corrected by Cs signal.

The depth profiles comparing the three different samples are shown in Figures 3A–3C. Figures 3A–3C show the migration of Pb, MA, and Br comparing the samples containing Li (blue), Na (red), and K (green). Figure 3D shows the profile distribution of the alkali cations: Li^+, Na^+, and K^+, showing how these three alkalis are also present at the perovskite surface. The effect of doping alkalis as the penetration barrier to perovskite ion diffusion concerning Pb, MA, and Br is shown with a clear trend. A homogeneous distribution of the perovskite ions is presented in the perovskite film (around 50 s after beginning the sputtering process). However, when we go deeper into the films, reaching the perovskite/mesoporous TiO_2 interface, inward diffusion of perovskite ions (Pb, MA, and Br) into the interface is detected.[31] Thus, the ETL/perovskite interfacial layer is permeable for the diffusion of Pb, MA, and Br. For the devices with Na interlayers (in red), the inward diffusion of the ions is effectively reduced, followed by the samples containing Li (blue) and K (green), being the latest one with more feasibility to allow perovskite ions to migrate. Thus, the inserted Na interlayer seems to have a robust impenetrability as an ion diffusion barrier. This gives us the trend of the facility of perovskite ions to migrate toward the interface as follows: K > Li > Na; perfectly matching with the trend obtained for the V_{oc} values: K < Li < Na. The fewer the perovskite ions at the interface, the lower the recombination and the higher the V_{oc}. This result alludes to the noteworthy effect of Na reducing the recombination processes related to the elimination of the NC and increase in the recombination resistance (R_{rec}) that we saw in the IS analysis.

Then, the ToF-SIMS explains the interfacial behavior seen through the IS analysis at the low-frequency domain. The reduction of recombination processes related to ionic

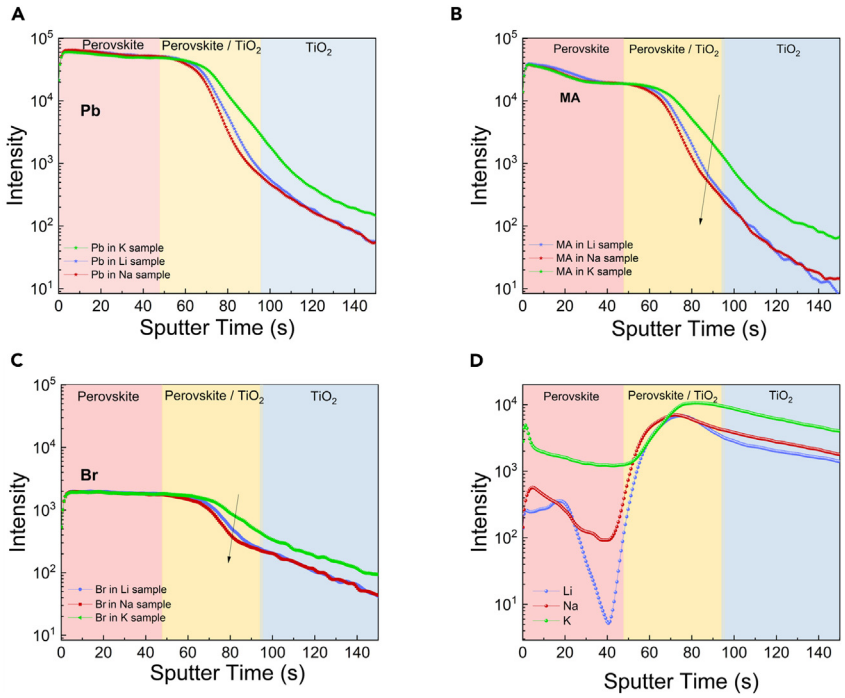

Figure 3. Bulk characterization: ToF-SIMS

(A–C) ToF-SIMS analysis showing the depth profile from the surface to the interface of the different perovskite ions (A) Pb, (B) MA, and (C) Br in each of the samples under study: containing Li, Na, or K. (D) Depth profile of the alkalis into the different layers.

migration and NC is due to a retarded ionic migration carried out by Na. To further investigate this effect, we performed XPS on each sample containing Li, Na, and K. This technique can also be used to further analyze the stability of the material[32,33]; thus, we use aged samples to perform the experiment. The core level peaks of Pb, Br, C, and N, which are attributed to the elements forming the PVK, are shown in Figure 4.

In Figure 4A, the core level peaks of Pb 4f show the corresponding perovskite Pb peak at ~138.9 eV for all the samples, together with a second peak at ~136.9 eV, which is identified as the metallic Pb^0 confirming the aging of the samples.[34] It is important to remember that all samples were analyzed without any encapsulation and at room conditions. The Br 3d, C 1s, and N 1s core level spectra have binding energies at around 69.0, 286.0, and 402.6 eV, respectively. All these peaks' position corresponds to the $CH_3NH_3PbBr_3$ PVK.[35,36] The Pb 4f and Br 3d peaks are shifted to lower binding energy for the Na samples with respect to the reference sample, whereas the position of the N 1s peak is shifted to higher binding energy. The opposite shifts in N 1s compared with Br 3d, would be caused by a strong chemical interaction between the organic compound MA and the Na. The interaction between the Na and organic compounds matches with the corresponding ToF-SIMS profile of MA, presenting reduced diffusion toward the interface. In addition, when we observe the composition extracted from the XPS fitting analysis (Table S2), a greater amount of organic compound of perovskite is found in the Na sample.

This interaction between Na and MA compounds can also explain the reduced recombination resistance in IS. In fact, the impact on the dielectric capacitance, related to bulk properties, can also be explained by this interaction.

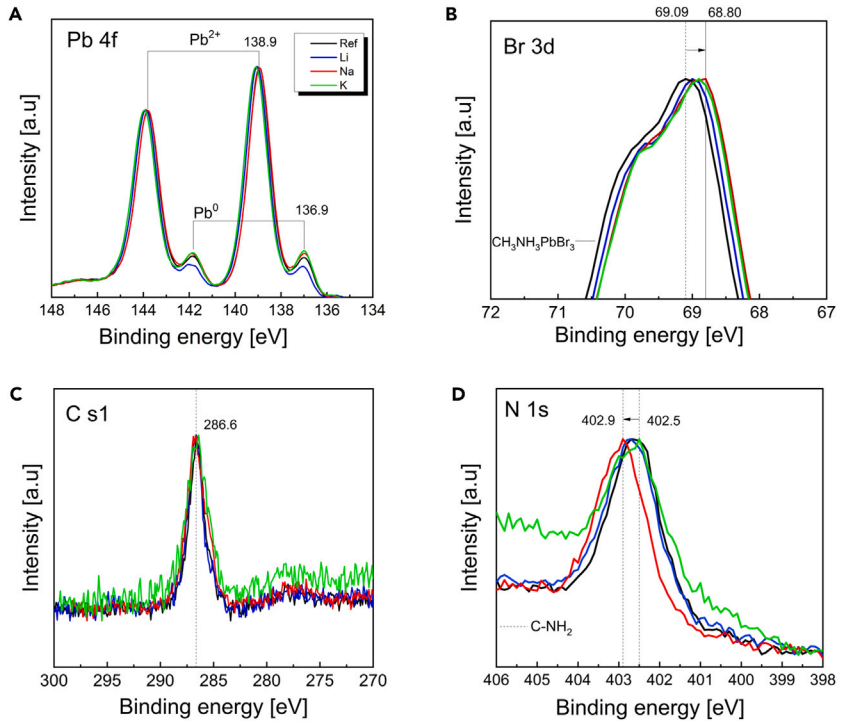

Figure 4. Bulk characterization: XPS analysis

XPS spectra of (A) Pb 4f, (B) Br 3d, (C) C 1s, and (D) N 1s peaks of un-doped (Ref-black), Li-doped (blue), Na-doped (red), and K-doped (green).

Mechanism proposed

In a recent publication by Suárez et al.,[37] the binding of alkali cations with small neutral ligands such as H_2O, NH_3, and CH_3NH_2 has been extensively studied. They suggest that the trend observed in alkali cations forming complexes with monovalent cations and neutral ligands, with "O" as the donor atom, exhibits a consistent trend of increasing Δq (charge transfer ability) from Li(I) to Na(I) to K(I). However, when "N" and "S" act as donors, as in the case of CH_3NH_2, this trend shifts to Na(I) > Li(I) > K(I).

Additionally, in a paper by Ceratti et al.,[38] which demonstrates proton diffusion in halide PVKs, an equilibrium has been established involving hydrogen, methylamine, and methylammonium within the PVK.

$$K_a = \frac{[H^+][CH_3NH_2]}{[CH_3NH_3^+]} \quad \text{(Equation 2)}$$

They have shown that the presence of Pb^{2+}, acting as a Lewis acid, promotes further dissociation of $CH_3NH_3^+$, releasing H^+ and forming a complex with CH_3NH_2 (Pb-N), leading to the stabilization of these species. It has been observed on multiple occasions that exposing hybrid perovskite cells to small amounts of water or methylamine improves their performance. They proposed that introducing proton vacancies and enhancing proton diffusivity can enhance the electronic quality of the material. This is because migrating protons can neutralize harmful charged defects present in the polycrystalline thin films used in devices.

Considering the presence of alkali cations in our experiment and considering the findings presented by Suárez et al.,[37] it is highly plausible that an interaction between alkali cations and CH_3NH_2 occurs, following the observed trend in our results,

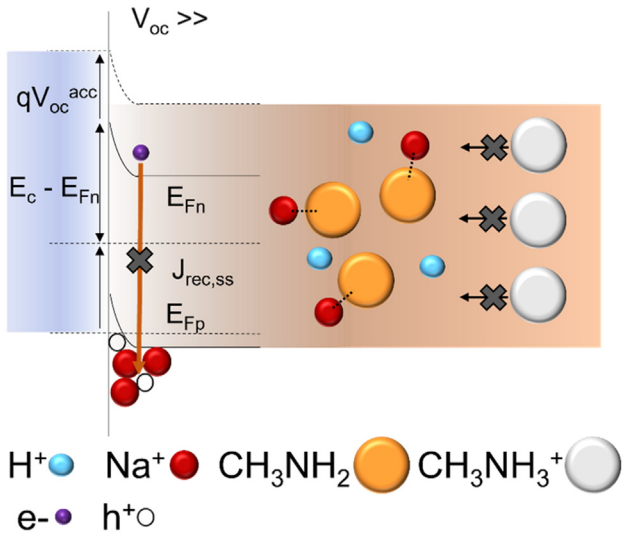

Figure 5. Schematic representation of the mechanism proposed

Energy band diagram of the accumulation zone at the perovskite near the ETL/perovskite interface in open circuit conditions. Here $J_{rec,ss}$ represents purely surface recombination between carriers (holes) located at the interfacial accumulation zone and how the Na cation avoids the accumulation of holes minimizing the interfacial recombination. In this model part of V_{oc} is built up at the interface because of the formation of the hole accumulation zone V_{oc}^{acc}, as previously reported,[21] represented here as an offset in the vacuum level. E_c is the perovskite conduction band and E_{Fn} and E_{Fp} correspond to the Fermi levels. Notice that the electrostatic interaction between Na-CH_3NH_2 impedes the migration of $CH_3NH_3^+$ toward the interface.

where Na exhibits the strongest interaction with CH_3NH_2, as confirmed by XPS. Then, if Na is strongly interacting with CH_3NH_2, the equilibrium (1) is less displaced to the reactants, favoring the photovoltaic performance of the cells. This interaction could be responsible for the effects found also in ToF-SIMS and the IS. We propose that this electrostatic interaction (Figure 5) could potentially account for the observed V_{oc} results and the corresponding trend: Na > Li > K.

The observed trend in V_{oc} concerning the presence of alkali elements in perovskite devices has also been confirmed using the well-established $MAPbI_3$ formulation (refer to Figure S9). This validation further bolsters the hypothesis presented here and enhances its applicability across various scenarios.

Conclusions

In this study, we conducted a systematic analysis of the effects of different alkali metals as dopants in the wide band-gap perovskite, $MAPbBr_3$. Our goal was to investigate the reasons behind the observed improvements in the PSCs photovoltage with alkali metals such as Li, Na, and K. A comprehensive analysis of morphology, bulk properties, and optoelectronic properties was conducted using various techniques including XRD, UV-Abs, PL, TRPL, ToF-SIMS, XPS, OCP, CV, and IS. All the data consistently demonstrated the same trend for the V_{oc} values: Na > Li > K, reaching an exceptional photovoltage of 1.6503 V for Na sample. This is accompanied by reduced hysteresis and elimination of NC. The reasons for this trend were revealed through several techniques. ToF-SIMS depth profiling showed a significant reduction in perovskite ionic migration especially for Na sample. This ability to hinder ionic migration was confirmed by XPS results, which indicated a higher binding energy in the N s1 spectra and a negative shift in the Br 3d spectra for the Na-doped sample compared with the reference, suggesting a strong electrostatic interaction between Na and CH_3NH_2 compounds. This interaction may

play a crucial role in the observed impedance results. Higher R_{rec} values were associated with improved bulk properties and reduced defect densities. NC was present in Li, K, and reference cells, but not in the Na-doped sample, indicating a reduction in interfacial recombination pathways, leading to improved V_{oc}. Furthermore, the dielectric capacitance was modified in the presence of Na, possibly due to the electrostatic interaction between Na and CH_3NH_2. We believe that the findings of this study will contribute to a better understanding of ionic modulation in PVKs and offer new possibilities for non-photovoltaic devices such as memristors, which are governed by ionic motion.

EXPERIMENTAL PROCEDURES

Resource availability

Lead contact

Further information and requests for resources should be directed to and will be fulfilled by the lead contact, Clara Aranda Alonso (clara.alonso@ipv.uni-stuttgart.de).

Materials availability

This study did not generate new unique materials.

Data and code availability

All data are presented in the paper or supplemental information, and no standardized datasets were generated during this study.

Fabrication of $MAPbBr_3$ solar cells

Deposition of electron transport layer (ETL)

FTO substrates were partially etched with zinc powder and HCl (2 M), cleaned by ultrasonication in Hellmanex detergent, rinsed with Milli-Q water and in a solution of ethanol:isopropanol (1:1 v/v). Prior to the deposition of TiO_2, compact layer substrates were treated in a UV-O_3 cleaner for 10 min. The TiO_2-blocking layer was deposited by aerosol spray pyrolysis at 450°C, using a commercial titanium diisopropoxide bis(acetylacetonate) solution (75% in 2propanol, Sigma-Aldrich) diluted in ethanol (1:9, v/v) as the precursor, with oxygen as carrier gas. The spray was performed with a total volume of 5 mL (approximately) of the previous solution, made by 3-step spraying of 6 s each and waiting 30 s between steps. The mesoporous layer was deposited by spin-coating at 2,000 rpm for 10 s followed by 100°C for 10 min. A 100 μL diluted paste in ethanol (1:5, weight ratio) of Dyesol 30-NRD was used. Devices were thermally treated in an oven under ambient atmosphere, using the following steps: 370°C for 20 min with 40 min ramp time, 470°C for 10 min with 5 min ramp time, and 500°C for 20 min.

Lithium, sodium, and potassium treatment

Before the deposition of perovskite films, three different solutions of 20 mg/mL containing Li, sodium, and potassium bis (trifluoromethylsulfonyl) imide in acetonitrile were prepared and deposited separately on the top of each device by spin-coating at 3,000 rpm (2,000 ac) for 10 s, followed by thermal treatment at 450°C for 30 min. All materials were purchased from Sigma-Aldrich.

Perovskite film deposition

$MAPbBr_3$ film was deposited, inside a glove box, using a 1-step deposition method. 1.4 M $PbBr_2$ precursor solution was prepared in N,N-dimethylformamide (DMF) and dimethylsulphoxide (DMSO) without stirring at 80°C for 20 min until complete dissolution. After cooling down at room temperature, this solution was mixed with MABr powder to obtain a final concentration of 1.4 M MABr. $MAPbBr_3$ solution was deposited by two ramps of the spin-coating method: 1,000 rpm for 10 s and 4,000 rpm for 40 s, using

toluene as an anti-solvent during the second ramp. This was followed by annealing at 100°C for 30 min to obtain a shiny and homogeneous film.

Deposition of HTL and external contact

A solution of Spiro-OMeTAD as HTL was prepared by dissolving 72.3 mg of (2,2′,7,7′-tetrakis(N,N′-di-pmethoxyphenylamine)-9,9′-spirobifluorene) in 1 mL of chlorobenzene, 28.8 μL of 4-tert-butylpyridine, and 17.5 μL of a stock solution of 520 mg/mL of Li bis-(trifluoromethylsulfonyl) imide in acetonitrile, as additives. Perovskite film was then covered with the HTL solution by dynamically spin-coating at 4,000 rpm, 800 rpm/s of acceleration for 30 s. Finally, 80 nm of gold was thermally evaporated on top of the device as a back contact, using a commercial Univex 250 chamber, from Oerlikon Leybold Vacuum.

Characterization of perovskite films and solar cells

UV-vis absorption spectra

Absorption spectra were recorded by a Cary 500 Scan VARIAN spectrophotometer in the 250–800 nm wavelength range.

SEM

The morphology of the films was observed using SEM CrossBeam 550 field emission scanning electron microscope from Carl Zeiss Microscopy.

Optoelectronic measures

For photovoltaic measures, a SINUS-70 solar simulator from WaveLabs comprising 21 LEDs of different wavelengths was used, adjusting the light intensity to 100 mW cm^{-2} using a calibrated Si-094 solar cell from Fraunhofer Institute for Solar Energy Systems ISE, adapted to a KG5 filter for thin films. Calibration of the reference cell was done the same year the measurements were performed. Devices were measured using a black mask to define an active area of 0.16 cm^2. *jV* curves were measured in reverse and forward bias at a scan rate of 50 mV s^{-1} under room conditions of temperature (25°C) and humidity (30% relative humidity [RH]). Impedance spectroscopy measures were performed using an Autolab potentiostat GSTT302N at open-circuit conditions under 1 sun, in a range of frequencies between 1 MHz to 1 mHz, with a voltage perturbation amplitude of 20 mV.

Photoluminescence

Measurements were collected by a PerkinElmer LAMBDA 1050, using 405 nm of excitation source.

XRD

XRD was performed in Bragg-Brentano geometry, collecting a single spectrum and using Cu Kα1 radiation on an Empyrean PANanalytical powder diffractometer. (Cu Kα, wavelength λ = 1.5406 Å.)

ToF-SIMS

The measurements were performed using a ToF-SIMS 5 device from IONTOF company, employing a LMIG with the following parameters: primary beam: Bi^+, 30 keV, 50 × 50 μm^2, 128 × 128 $Pixel^2$, positive polarization. Secondary beam: Cs, 1 keV, 200 × 200 μm^2, 5 frames. To minimize sputter and surface charging effects on signal intensity, measured signals were corrected by Cs signal.

SUPPLEMENTAL INFORMATION

Supplemental information can be found online at https://doi.org/10.1016/j.joule.2023.11.011.

ACKNOWLEDGMENTS

C.A.A. thanks the Helmholtz Young Investigator Group FRONTRUNNER. M.R. acknowledges the Alexander von Humboldt foundation for the research fellowship. M.S. thanks the German Research Foundation (DFG) for funding (SPP2196, GRK 2642). M.S. acknowledges funding by ProperPhotoMile. Project ProperPhotoMile is supported under the umbrella of SOLAR-ERA.NET Cofound 2 by The Spanish Ministry of Science and Education and the AEI under the project PCI2020-112185 and CDTI project number IDI-20210171; the Federal Ministry for Economic Affairs and Energy based on a decision by the German Bundestag project number FKZ 03EE1070B and FKZ 03EE1070A and the Israel Ministry of Energy with project number 220-11-031. SOLAR-ERA.NET is supported by the European Commission within the EU Framework Programme for Research and Innovation HORIZON 2020 (Cofound ERA-NET Action, no. 786483). M.S. acknowledges funding from the European Union under the Horizon Europe programme (ERC, LOCAL-HEAT, grant agreement no. 101041809). Views and opinions expressed are however those of the author(s) only and do not necessarily reflect those of the European Union or the European Research Council. Neither the European Union nor the granting authority can be held responsible for them. C.A.A. also greatly thanks the following researchers: Dr. Cristina Momblona from ICMUV (Instituto de Ciencia de los Materiales de la Universidad de Valencia), Dr. Theresa Magorian, and specially Dr. Wolfram Hempel from ZSW (Zentrum für Sonnenenergie und Wasserstoff-Forschung) for their invaluable help in performing the instrumental techniques of XRD, SEM, and ToF-SIMS/XPS, respectively. Special thanks to Dr. Renán Escalante for his helpful input with the table of contents of this manuscript.

AUTHOR CONTRIBUTIONS

C.A.A. provided the original idea, developed the experimental and characterization design, fabricated the perovskite devices, carried out the photovoltaic and impedance measurements, performed the data analysis, built the figures, and wrote the manuscript. A.O.A. carried out the impedance spectra fittings and calculations, contributing to data analysis and discussion. V.S.C. performed the TRPL measurements and its data analysis. C.D. contributed to the XPS analysis and helped with the writing of that part. M.R. contributed to the TRPL discussion. M.S. supervised the research and discussion of results, validating, reviewing, and improving the manuscript.

DECLARATION OF INTERESTS

The authors declare no competing interests.

Received: March 13, 2023
Revised: May 26, 2023
Accepted: November 20, 2023
Published: December 13, 2023

REFERENCES

1. Snaith, H.J., Abate, A., Ball, J.M., Eperon, G.E., Leijtens, T., Noel, N.K., Stranks, S.D., Wang, J.T.-W., Wojciechowski, K., and Zhang, W. (2014). Anomalous hysteresis in perovskite solar cells. J. Phys. Chem. Lett. *5*, 1511–1515.

2. Tress, W., Marinova, N., Moehl, T., Zakeeruddin, S.M., Nazeeruddin, M.K., and Grätzel, M. (2015). Understanding the rate-dependent J-V hysteresis, slow time component, and aging in CH3NH3PbI3 perovskite solar cells: the role of a compensated electric field. Energy Environ. Sci. *8*, 995–1004.

3. Chen, B., Yang, M., Zheng, X., Wu, C., Li, W., Yan, Y., Bisquert, J., Garcia-Belmonte, G., Zhu, K., and Priya, S. (2015). Impact of capacitive effect and ion migration on the hysteretic behavior of perovskite solar cells. J. Phys. Chem. Lett. *6*, 4693–4700.

4. Green, M.A. (2012). Radiative efficiency of state-of-the-art photovoltaic cells. Prog. Photovolt. Res. Appl. *20*, 472–476.

5. Tress, W., Correa Baena, J.P., Saliba, M., Abate, A., and Graetzel, M. (2016). Inverted current–voltage hysteresis in mixed perovskite solar cells: polarization, energy barriers, and defect recombination. Adv. Energy Mater. *6*, 1600396.

6. Richardson, G., O'Kane, S.E.J., Niemann, R.G., Peltola, T.A., Foster, J.M., Cameron, P.J., and Walker, A.B. (2016). Can slow-moving ions explain hysteresis in the current–voltage curves of perovskite solar cells? Energy Environ. Sci. *9*, 1476–1485.

7. Saliba, M., Matsui, T., Seo, J.-Y., Domanski, K., Correa-Baena, J.-P., Nazeeruddin, M.K., Zakeeruddin, S.M., Tress, W., Abate, A., Hagfeldt, A., et al. (2016). Cesium-containing triple cation perovskite solar cells: improved stability, reproducibility and high efficiency. Energy Environ. Sci. *9*, 1989–1997.

8. Xu, C., Chen, X., Ma, S., Shi, M., Zhang, S., Xiong, Z., Fan, W., Si, H., Wu, H., Zhang, Z., et al. (2022). Interpretation of rubidium-based perovskite recipes toward electronic passivation and ion-diffusion mitigation. Adv. Mater. *34*, e2109998.

9. Saliba, M., Matsui, T., Domanski, K., Seo, J.Y., Ummadisingu, A., Zakeeruddin, S.M., Correa-Baena, J.P., Tress, W.R., Abate, A., Hagfeldt, A., et al. (2016). Incorporation of rubidium cations into perovskite solar cells improves photovoltaic performance. Science *354*, 206–209.

10. Kim, S.-G., Li, C., Guerrero, A., Yang, J.-M., Zhong, Y., Bisquert, J., Huettner, S., and Park, N.-G. (2019). Potassium ions as a kinetic controller in ionic double layers for hysteresis-free perovskite solar cells. J. Mater. Chem. A *7*, 18807–18815.

11. Peng, W., Aranda, C., Bakr, O.M., Garcia-Belmonte, G., Bisquert, J., and Guerrero, A. (2018). Quantification of ionic diffusion in lead halide perovskite single crystals. ACS Energy Lett. *3*, 1477–1481.

12. Bisquert, J. (2000). Influence of the boundaries in the impedance of porous film electrodes. Phys. Chem. Chem. Phys. *2*, 4185–4192.

13. Zarazua, I., Han, G., Boix, P.P., Mhaisalkar, S., Fabregat-Santiago, F., Mora-Seró, I., Bisquert, J., and Garcia-Belmonte, G. (2016). Surface recombination and collection efficiency in perovskite solar cells from impedance analysis. J. Phys. Chem. Lett. *7*, 5105–5113.

14. Karlsson, M., Yi, Z., Reichert, S., Luo, X., Lin, W., Zhang, Z., Bao, C., Zhang, R., Bai, S., Zheng, G., et al. (2021). Mixed halide perovskites for spectrally stable and high-efficiency blue light-emitting diodes. Nat. Commun. *12*, 361.

15. Kausar, A., Sattar, A., Xu, C., Zhang, S., Kang, Z., and Zhang, Y. (2021). Advent of alkali metal doping: a roadmap for the evolution of perovskite solar cells. Chem. Soc. Rev. *50*, 2696–2736.

16. Cao, J., Tao, S.X., Bobbert, P.A., Wong, C.-P., and Zhao, N. (2018). Interstitial occupancy by extrinsic alkali cations in perovskites and its impact on ion migration. Adv. Mater. *30*, e1707350.

17. Aranda, C., Guerrero, A., and Bisquert, J. (2019). Ionic effect enhances light emission and the photovoltage of methylammonium lead bromide perovskite solar cells by reduced surface recombination. ACS Energy Lett. *4*, 741–746.

18. Alvarez, A.O., Arcas, R., Aranda, C.A., Bethencourt, L., Mas-Marzá, E., Saliba, M., and Fabregat-Santiago, F. (2020). Negative capacitance and inverted hysteresis: matching features in perovskite solar cells. J. Phys. Chem. Lett. *11*, 8417–8423.

19. Heo, J.H., You, M.S., Chang, M.H., Yin, W., Ahn, T.K., Lee, S.-J., Sung, S.-J., Kim, D.H., and Im, S.H. (2015). Hysteresis-less mesoscopic CH3NH3PbI3 perovskite hybrid solar cells by introduction of Li-treated TiO2 electrode. Nano Energy *15*, 530–539.

20. Saidaminov, M.I., Abdelhady, A.L., Murali, B., Alarousu, E., Burlakov, V.M., Peng, W., Dursun, I., Wang, L., He, Y., Maculan, G., et al. (2015). High-quality bulk hybrid perovskite single crystals within minutes by inverse temperature crystallization. Nat. Commun. *6*, 7586. https://www.nature.com/articles/ncomms8586#supplementary-information.

21. Zarazua, I., Bisquert, J., and Garcia-Belmonte, G. (2016). Light-induced space-charge accumulation zone as photovoltaic mechanism in perovskite solar cells. J. Phys. Chem. Lett. *7*, 525–528.

22. Ravishankar, S., Almora, O., Echeverría-Arrondo, C., Ghahremanirad, E., Aranda, C., Guerrero, A., Fabregat-Santiago, F., Zaban, A., Garcia-Belmonte, G., and Bisquert, J. (2017). Surface polarization model for the dynamic hysteresis of perovskite solar cells. J. Phys. Chem. Lett. *8*, 915–921.

23. Berruet, M., Pérez-Martínez, J.C., Romero, B., Gonzales, C., Al-Mayouf, A.M., Guerrero, A., and Bisquert, J. (2022). Physical model for the current–voltage hysteresis and impedance of halide perovskite memristors. ACS Energy Lett. *7*, 1214–1222.

24. Gonzales, C., Guerrero, A., and Bisquert, J. (2022). Transition from capacitive to inductive hysteresis: A neuron-style model to correlate I–V curves to impedances of metal halide perovskites. J. Phys. Chem. C *126*, 13560–13578.

25. Jiang, Y., Feng, Y., Sun, X., Qin, R., and Ma, H. (2019). Identifying inverted-hysteresis behavior of CH3NH3PbI3−xClx planar hybrid perovskite solar cells based on external bias precondition. J. Phys. D: Appl. Phys. *52*, 385501.

26. Lan, D. (2020). The physics of ion migration in perovskite solar cells: insights into hysteresis, device performance, and characterization. Prog. Photovolt. Res. Appl. *28*, 533–537.

27. Almora, O., Zarazua, I., Mas-Marza, E., Mora-Sero, I., Bisquert, J., and Garcia-Belmonte, G. (2015). Capacitive dark currents, hysteresis, and electrode polarization in lead halide perovskite solar cells. J. Phys. Chem. Lett. *6*, 1645–1652.

28. Bisquert, G., Mora-Sero, I., and J.G.-B.. (2016). Characterization of capacitance, transport and recombination parameters in hybrid perovskite and organic solar cells. In Unconventional Thin Film Photovoltaics (The Royal Society of Chemistry, Cambridge), pp. 57–106.

29. Ghahremanirad, E., Bou, A., Olyaee, S., and Bisquert, J. (2017). Inductive loop in the impedance response of perovskite solar cells explained by surface polarization model. J. Phys. Chem. Lett. *8*, 1402–1406.

30. Bisquert, J. (2022). Interpretation of the recombination lifetime in halide perovskite devices by correlated techniques. J. Phys. Chem. Lett. *13*, 7320–7335.

31. Wu, S., Chen, R., Zhang, S., Babu, B.H., Yue, Y., Zhu, H., Yang, Z., Chen, C., Chen, W., Huang, Y., et al. (2019). A chemically inert bismuth interlayer enhances long-term stability of inverted perovskite solar cells. Nat. Commun. *10*, 1161.

32. Zhidkov, I.S., Poteryaev, A.I., Kukharenko, A.I., Finkelstein, L.D., Cholakh, S.O., Akbulatov, A.F., Troshin, P.A., Chueh, C.-C., and Kurmaev, E.Z. (2020). XPS evidence of degradation mechanism in CH3NH3PbI3 hybrid perovskite. J. Phys. Condens. Matter *32*, 095501.

33. Lin, W.-C., Lo, W.-C., Li, J.-X., Wang, Y.-K., Tang, J.-F., and Fong, Z.-Y. (2021). In situ XPS investigation of the X-ray-triggered decomposition of perovskites in ultrahigh vacuum condition. npj Mater. Degrad. *5*, 13.

34. Das, C., Wussler, M., Hellmann, T., Mayer, T., and Jaegermann, W. (2018). In situ XPS study of the surface chemistry of MAPI solar cells under operating conditions in vacuum. Phys. Chem. Chem. Phys. *20*, 17180–17187.

35. Luo, J., Zhang, Y., Matios, E., Wang, P., Wang, C., Xu, Y., Hu, X., Wang, H., Li, B., and Li, W. (2022). Stabilizing sodium metal anodes with surfactant-based electrolytes and unraveling the atomic structure of interfaces by cryo-TEM. Nano Lett. *22*, 1382–1390.

36. Wang, K., Ecker, B., and Gao, Y. (2021). Photoemission studies on the environmental stability of thermal evaporated MAPbI3 thin films and MAPbBr3 single crystals. Energies *14*, 2005.

37. López, R., Díaz, N., and Suárez, D. (2020). Alkali and alkaline-earth cations in complexes with small bioorganic ligands: ab initio benchmark calculations and bond energy decomposition. ChemPhysChem *21*, 99–112.

38. Ceratti, D.R., Zohar, A., Kozlov, R., Dong, H., Uraltsev, G., Girshevitz, O., Pinkas, I., Avram, L., Hodes, G., and Cahen, D. (2020). Eppur si muove: proton diffusion in halide perovskite single crystals. Adv. Mater. *32*, e2002467.